



Effect of Different Annealing Techniques on CIGS Deposited Using One-Step Single-Target Sputtering

Sachin V. Desarada¹ · Kalyan B. Chavan² · Nandu B. Chaure¹

Received: 29 August 2022 / Accepted: 14 February 2023 / Published online: 8 March 2023
© The Minerals, Metals & Materials Society 2023

Abstract

The post-processing of CuInGaSe₂ (CIGS) thin films deposited using a single-target sputtering method was studied. Post-processing annealing was performed in a traditional muffle furnace and rapid thermal processing (RTP) tube furnace. The samples were annealed at 450°C for 10 min in a muffle furnace and subsequently quenched, whereas multiple quenching cycles were performed in RTP. The structural, optical, elemental, and morphological properties of the samples were analyzed. The obtained XRD data were refined using the Rietveld refinement algorithm, which showed that the *c/a* value approaches the ideal tetragonal crystal structure in the RTP-treated sample and that the crystallinity of the RTP-treated sample was better than that of the traditional furnace-annealed samples. Optical measurements showed increased absorbance values in the RTP-treated samples compared with the furnace-annealed samples. Bandgap was estimated to be 1.30 eV, 1.22 eV, and 1.18 eV for as-deposited, furnace annealing, and RTP-treated samples. Our experiment showed that better results were obtained in the RTP-treated samples, with a similar parameter used for annealing.

Keywords CIGS · RF sputtering · rapid thermal annealing · structural properties

Introduction

Thin-film polycrystalline absorber materials have gained attention for use in solar cells in recent years owing to their promising results for high-efficiency thin-film solar cells (TFSC). CuInGaSe₂ (CIGS), CdTe, and Cu₂ZnSnS₄ (CZTS) semiconductor-based solar cells have been studied extensively because of their properties such as wide bandgap within the visible region, high absorption coefficient, and economical solution processing method.¹ Among these, CIGS has been considered a promising material for thin-film solar cells because the energy bandgap of CIGS semiconductors can be tuned in the range of 1.05 eV to 1.65 eV by changing the stoichiometry of indium (In) to gallium (Ga) of the sample (CuInSe₂ – 1.05 eV, CuGaSe₂ – 1.65 eV).² CIGS also has a large minority carrier diffusion length and high absorption coefficient ($\sim 10^5 \text{ cm}^{-1}$), allowing only

a few-micrometer-thick layer to absorb most of the solar radiation falling on the material.^{3,4} The efficiency gap between CIGS-based TFSC and traditional Si solar cells has decreased. For example, 22.6% efficient CIGS-based solar cells have been reported, and recently, 23.35% efficient lab-scale cells and 19.64% efficient modules were fabricated, which are efficient as traditional silicon solar cells.^{5,6}

CIGS layers can be deposited using vacuum and non-vacuum methods such as co-evaporation, sputtering, and electrodeposition.^{7–9} According to various reports, a post-annealing process was required to improve the crystallinity, grain size, and compactness of CIGS samples.^{10,11} Some of the literature reports are summarized and presented in Table III. Annealing under a selenium atmosphere is a well-developed technique for preparing CIGS thin films. However, owing to the toxicity of Se to the environment and human health, many researchers are exploring single-step deposition of CIGS without selenization.¹² Multi-stage deposition of CIGS involves the deposition of metallic Cu, In, and Ga species in the preferred order, followed by annealing in ambient selenium; this method can control the composition of polycrystalline CIGS thin films.^{13,14} CIGS is a polycrystalline structure that allows elemental doping using post-processing techniques at lower temperatures.

✉ Nandu B. Chaure
n.chaure@physics.unipune.ac.in

¹ Department of Physics, Savitribai Phule Pune University, Pune 411007, India

² Department of Physics, Ahmednagar College, Ahmednagar 414001, India

Ruddmann reported Na doping using a post-processing technique to introduce the Na doping in CIGS at 500°C, which was reported to alter the electronic properties of CIGS, similar approach adopted by He X. shows the doping can be achieved at a lower 300°C temperature.^{15,16} Traditionally, CIGS films were annealed inside a tubular furnace in a Se atmosphere¹⁷; however, multiple annealing techniques have been studied by researchers. For example, rapid thermal processing (RTP) was used on CuInSe₂ (CIS) under a Se atmosphere to develop large-area solar cells.¹⁸ Ray et al. introduced a rapid annealing method to process the CIGS thin films to control the Cu vacancies in the CIGS compound by improving the grain boundary defects by faster recrystallization of the sample.¹⁹ Kim et al. adopted an annealing technique using a continuous-wave Nd:YAG laser in ambient vacuum condition, in which p-type and n-type conductivity can be controlled by changing the laser power within the range of 2–3 W.²⁰ RTP has been used to heat materials at a higher heating rate, which can efficiently reduce low-temperature elemental interdiffusion. The effect of RTP treatment on electrodeposited CIS thin films was reported by Rohom et al., which showed an efficiency enhancement in RTP-treated samples.²¹

In this study, we investigated the impact of post-processing on a single-stage RF-sputtered CIGS layer. A modified RTP technique was used to process the as-sputtered samples without additional selenization. The samples were annealed in a muffle furnace (MF-annealed) and an RTP chamber (RTP-treated) to optimize the post-processing annealing technique for the CIGS thin film. A unique RTP profile with successive higher and lower annealing temperature was utilized. The structural and optical properties are reported to discuss the effect of post-processing on sputtered CIGS using different annealing techniques.

Experimental

The CIGS thin films were deposited on glass substrates using a single-target radio-frequency (RF) sputtering technique. The borosilicate glass substrates were cleaned with piranha acid cleaning solution and stored in isopropyl alcohol solution. Prior to deposition, the sputtering chamber was evacuated using a turbomolecular pump coupled with a backing rotary pump at a pressure of $\sim 10^{-5}$ mbar, and argon (Ar) gas was purged at a flow rate of 60 sccm. The CIGS sample was continuously deposited at 120 W RF power and a substrate temperature of 300°C for 30 min. For post-deposition processing, the samples were annealed at 450°C for 10 min in a muffle furnace and an RTP chamber in ambient air. The muffle furnace temperature was raised to 450°C, and the CIGS sample was placed and annealed for 10 min, after which the sample was quenched by placing it on the ceramic plate.

Another sample was annealed in an RTP furnace, where the sample underwent multiple heating and cooling techniques in 10 s, with the ramp rate set to 25°C/s and 10 s soak time. A schematic representation of the RTP cycle is shown in Fig. 1, where the ON/OFF ratio and soaking times are marked. The optical, structural, elemental, and morphological properties of the prepared samples were characterized. The structural properties were studied using x-ray diffraction (XRD) with a Bruker D8 Advance x-ray diffractometer with CuK α 0.154 nm radiation. XRD data were refined using the Rietveld refinement method to obtain lattice parameters and chemical composition using Profex software with a BGMN backend.²² The optical properties were measured using a JASCO V-770 ultraviolet–visible (UV–VIS) spectrophotometer. Raman spectra were acquired using a Renishaw inVia™ Raman spectrometer coupled with 532 nm laser excitation wavelength. The surface morphology was analyzed using a scanning electron microscope (SEM) (JEOL JSM-6360A), and the relative atomic concentration was obtained using energy-dispersive x-ray analysis (EDAX) with the module attached to the SEM instrument.

Results and Discussion

X-Ray Diffraction

Figure 2 shows the XRD patterns measured for the as-deposited sample a), annealed in a muffle furnace (MF) b), and rapid thermal processing (RTP)-treated sample c). Three peaks are observed in all the samples at about 27.7°, 44.2°, and 52.4°, which are identified to be (112), (220)/(204), and (312)/(116) diffraction plane of the tetragonal crystal structure of CIGS (JCPDS #00-035-1102). No peaks associated with the

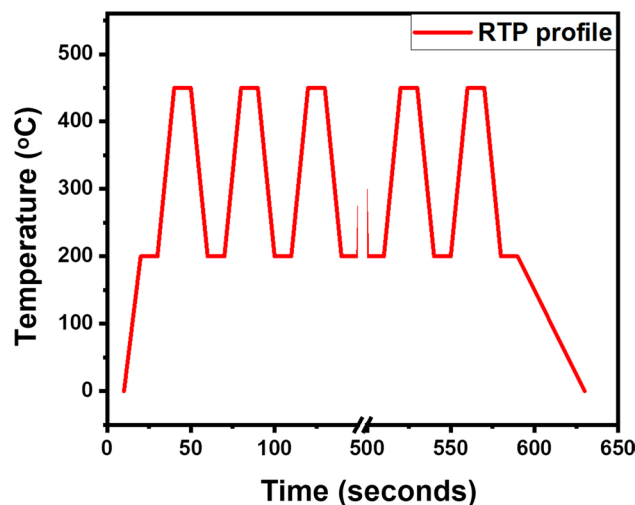


Fig. 1 Temperature cycle profile for RTP treatment.

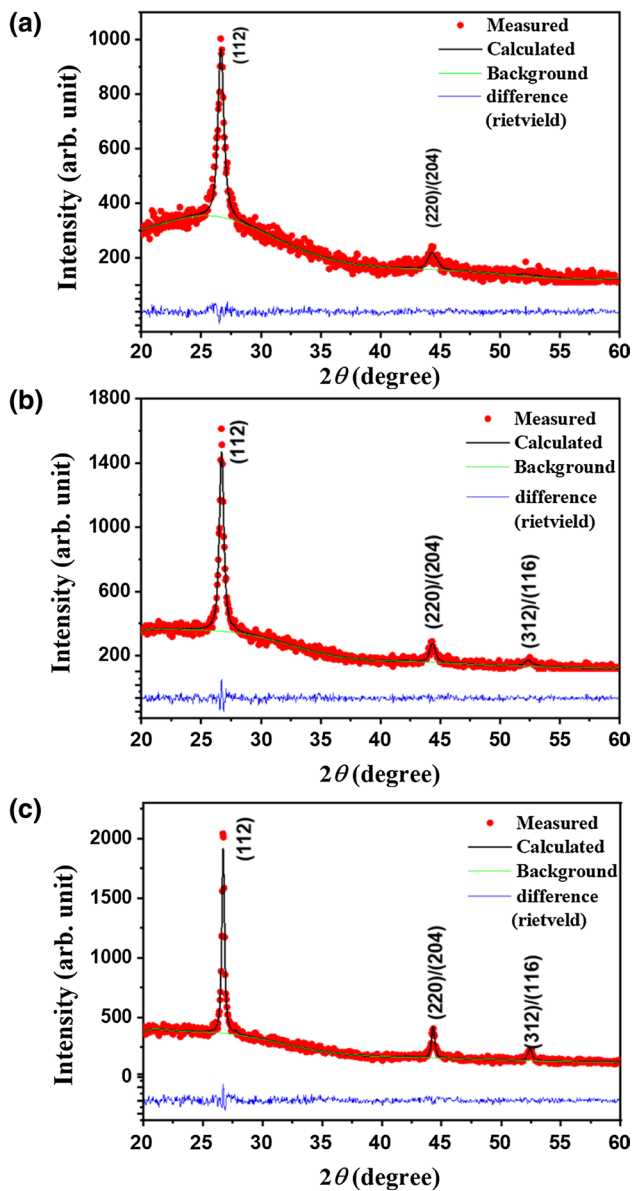


Fig. 2 XRD data measured and Rietveld-refined graph of as-deposited (a), MF-annealed (b), and RTP-treated sample (c).

secondary phases were observed, confirming the growth of a single quaternary CIGS phase. Figure 1 shows the XRD spectra along with the refined parameter obtained using Rietveld refinement with a good fit quality ($\chi^2 < 1.5$) to obtain the lattice parameter. The crystal size and strain can affect the width of the observed diffraction peaks in the XRD data. Using the full-width half-minima (FWHM) of the diffraction peak, the average crystallite size can be obtained using the Scherrer formula²³:

$$d = \frac{k\lambda}{\beta \cos\theta} \quad (1)$$

Table 1 Crystallite size and lattice parameters obtained by XRD analysis after Rietveld refinement

Samples	Crystallite size (nm)	Lattice parameters (nm) (Rietveld-refined structure)			Inter-planar spacing (112) (nm)
		a	c	c/a	
As-deposited	9.31	0.569	1.162	2.04	0.330
MF-annealed	17.06	0.574	1.159	2.02	0.332
RTP-treated	30.84	0.577	1.159	2.01	0.334

where d is the average crystallite size, k is the shape factor (0.9 for spherical shape), λ is the x-ray wavelength (1.543 Å), β is the FWHM of the (112) diffraction peak, and θ is the diffraction angle in radians. The calculation was performed on the Rietveld-refined data to accurately estimate the grain size, as shown in Table 1. The average crystallite size was found to increase in the annealed samples, indicating improved crystallinity of CIGS. The RTP-treated sample showed a larger crystallite size than the as-deposited and MF-annealed samples. The growth in the crystalline size of the RTP-treated samples was proposed to be associated with recrystallization owing to the multiple quenching cycles performed in the RPT, which promoted a higher growth rate compared to the single quenching cycle in the MF-annealed sample. For a perfect tetragonal crystal structure system, the lattice follows the $c = 2a$ relation. Table 1 also shows the lattice parameters a and c obtained from Rietveld refinement. We observed a decrease in the c/a ratio approaching a value of 2 for the annealed sample and the lowest for the RTP-treated sample, which suggests a tendency to recrystallize and from a perfect tetragonal crystal structure in the RTP-treated sample. Similar results were reported by Kim et al. for RTP on thermally evaporated CIGS layers, showing that CIGS crystals formed above 400°C, while recrystallization was observed above 480°C.²⁴ The average interplanar spacings (d) for the (112) plane were 0.330 nm, 0.332 nm, and 0.334 nm for the as-deposited, MF-annealed, and RTP-treated samples, respectively. Shih et al. reported a decrease in d in the range of 0.337–0.235 nm as a function of increasing Ga content; similar results were obtained by Soce et al.^{25,26} Our results revealed a minor change in d , which indicated a slight variation in Ga content.

UV–Vis–NIR Spectroscopy

Figure 3 shows the Tauc plot and absorption graph in the inset of the UV–Vis–near-infrared (NIR) spectra. The optical energy bandgap can be estimated from a Tauc plot using the energy-dependent absorption coefficient (α) by the following equation²⁷:

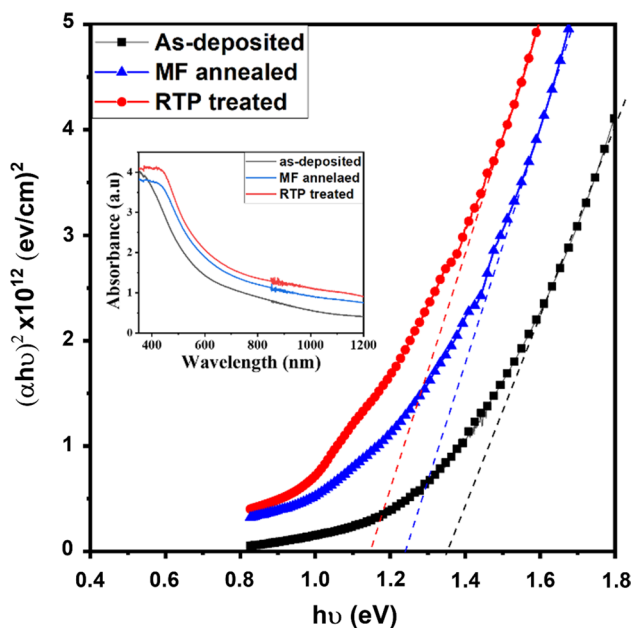


Fig. 3 Tauc plot obtained using UV–Vis–NIR spectroscopy (inset shows the absorption spectra).

$$(\alpha \cdot h\nu)^{\frac{1}{r}} = \beta(h\nu - E_g) \quad (2)$$

where α is the absorption coefficient, β is the tailing factor, h is Planck's constant, ν is the frequency, E_g is the energy bandgap, and r is the power factor that depends on the transition mode ($1/2$ for direct band transitions). Figure 2 shows the $(\alpha h\nu)^2$ versus $(h\nu)$ plot, where the energy bandgap can be estimated by extrapolating the straight line on the energy axis. The bandgaps of the as-deposited, MF-annealed, and RTP-treated samples were estimated as 1.31, 1.21, and 1.18, respectively. The absorbance of the annealed samples increased, and the RTP-treated sample exhibited the highest absorbance value. A decrease in the energy bandgap upon annealing was attributed to the increase in particle size owing to the agglomeration of the small particles, thereby reducing the quantum confinement of electrons. The quantum confinement effect arises because of the concentration of the localized energy state and is more prominent in bulk materials than in smaller crystals. The annealing process increased the crystallite size, increasing the density of the localized energy states by reducing the defect density in the crystal and reducing the confinement effect. The energy bandgap of the CIGS semiconductor also depends on the Ga/(In+Ga) ratio; the reduction in the bandgap of the annealed samples could also be a result of the reduction in Ga, and a slight change in Ga was also evident from the XRD studies. We did not find any significant change in the

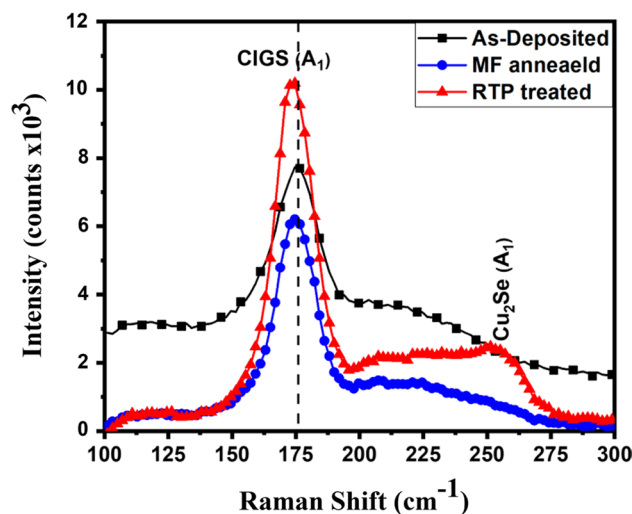


Fig. 4 Raman spectra acquired using 532 nm laser for as-deposited, MF-annealed, and RTP-treated samples.

Ga content in the crystal structure, which shows that the significant contribution to bandgap reduction is from the change in crystallite size.

Raman Spectroscopy

Figure 4 shows the Raman spectra of the as-deposited, MF-annealed, and RTP-treated samples acquired using the 512 nm excitation wavelength laser. The intense peak at 176 cm^{-1} was assigned to the transverse optical A_1 mode of CIGS, which is the most substantial observed peak in related I-II-VI₂ chalcopyrite compounds. The A_1 mode of CIGS results from the vibration of Se anions with the rest of the cations, where two anions move in the x -direction antiparallel to each other, and the remaining two move in the y -direction in the same manner.²⁸ The position of A_1 shifts as the Ga content in the molecule decreases, and the peak shifts towards a higher wavelength as the Ga content increases in the CIGS.²⁹ Raman spectra for the as-deposited sample show a peak related to A_1 mode. The prominent A_1 peak shifted in the annealed sample, which indicates that the Ga content in the molecule decreased, as is also evident from the XRD analysis. A small shoulder peak attributed to approximately 252 cm^{-1} in the RTP-treated sample is associated with the A_1 mode of the Cu_2Se phase. Traces of the phase related to Cu–Se are not observed in the XRD analysis, which may be because the quantity of the Cu_2Se phase is very small and is formed at the surface. The intensity of the peak was found to increase in the annealed sample and was highest in the RTP-treated sample, which shows the increased crystallinity of the sample.

Scanning Electron Microscopy

Figure 5 shows the SEM micrographs and particle distribution bar charts at the bottom for the as-deposited and annealed samples. Compact and densely packed grain growth was observed. The data were processed using ImageJ software to obtain size and distribution information.³⁰ The as-deposited sample showed a non-uniform particle size over the surface, whereas the particle size distribution was enhanced after annealing. The average areas of the surface particles were estimated to be 25 nm, 83 nm, and 86 nm for the as-deposited, MF-annealed, and RTP-treated samples, respectively. Annealing the sample shows an improvement in average particle size as well as distribution, which may be due to the recrystallization of the sample upon heating. The particle size distribution histogram for the RTP-treated sample fitted with a Gaussian curve suggests more uniform distribution over the surface compared to other samples. No cracks were observed in the RTP sample even after multiple rapid cooling cycles. Table II lists the observed relative atomic concentrations of the samples. A significant change was observed in the content of Se, which decreased with annealing and was lowest in the RTP-treated sample, which might be due to the highly volatile nature of Se resulting in liberation from the sample at high temperatures. In contrast to the results obtained from the XRD and Raman analyses, we found an increase in the Ga/In ratio in the EDAX samples. This can be explained by the penetration depth of low-power x-ray used in EDAX analysis, where x-rays can only penetrate to a depth of a few nanometers, and thus the analysis reflects the surface properties of the material (Table III).

Conclusion

CIGS thin films were deposited using a single-step RF sputtering method. Post-processing in a traditional muffle furnace and modified RTP were studied and compared. Rietveld refinement of the XRD data revealed an improvement in crystallinity and the formation of a tetragonal crystal structure in the RTP-treated sample. The RTP-treated samples exhibit better crystallinity and c/a values near the ideal tetragonal crystal structure. The annealed sample shows a low bandgap, which might be due to the increase in the crystallite size, which promotes fewer defects and a high concentration of localized energy states. Raman analysis shows a slight shift in the A_1 mode peak, suggesting a reduction in the Ga/In ratio in the sample. We observed rectangular grains on the surface with increased size and uniformity in the annealed sample. A comparative study showed that the custom RTP technique could achieve similar results with reduced time. The study confirms that the effective use of RTP treatment on the CIGS sample, with multiple higher and lower heating steps, could achieve higher crystalline

Table II Relative atomic concentration in samples obtained by EDAX analysis

Samples	Relative atomic concentration (%)			
	Cu	In	Ga	Se
As-deposited	19.21	19.26	6.11	55.42
MF-annealed	18.93	20.06	6.05	54.96
RTP-treated	19.74	20.31	6.24	53.74

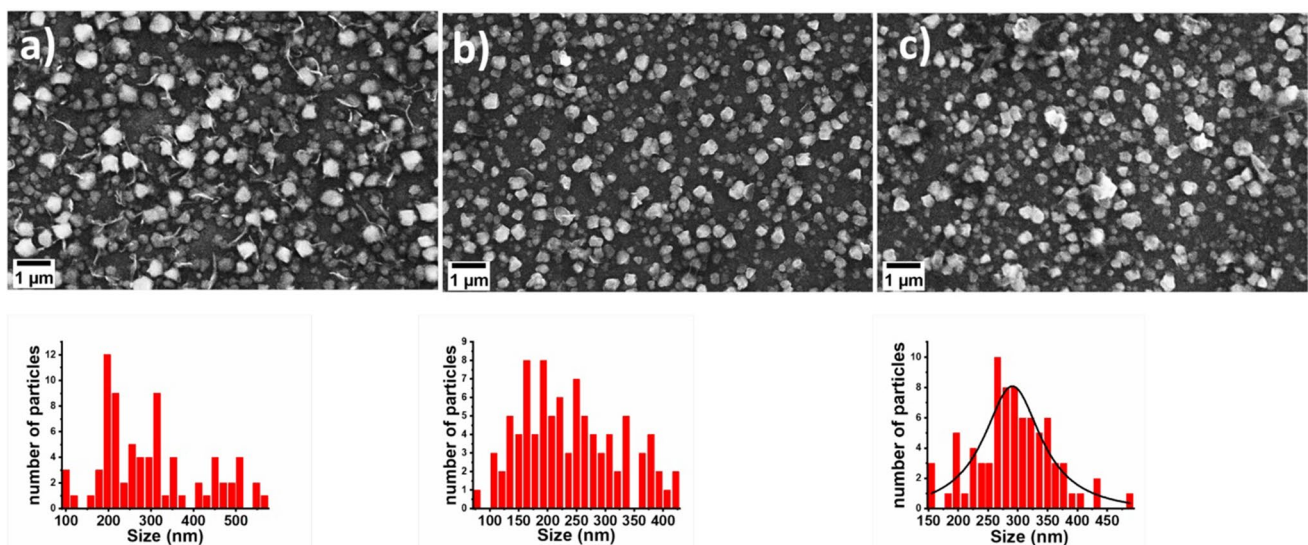


Fig. 5 SEM micrographs and particle size distribution histogram at the bottom of the as-deposited (a), MF-annealed (b), and RTP-treated samples (c).

Table III Reports from the literature on the effect of annealing on CIGS thin films

Sr. no.	Thin film deposition method		Post-processing technique			Average crystalline size (nm)	Energy bandgap (eV)	Ref
			Method	Temperature (°C)	Time (min)			
1	Sputtering		Selenization	450	30	40	1.2	18
2	Electrodeposition		Selenization	400	30	20	1.28	31
3	Co-evaporation		Selenization	560	50	40	–	32
4	Electrodeposition		Tube furnace	400	30	–	1.33	33
5	Sputtering		Annealed in sputtering chamber	550	30	20	–	34
6	Current study	Sputtering	MF-annealed	450	10	17	1.21	
7			RTP	450	10	31	1.18	

and uniform thin films compared to traditional annealing at similar temperature and time.

Acknowledgments The authors are grateful to SERB, New Delhi, for their financial support.

Conflict of interest The authors declare that they have no conflict of interest.

References

- F. Liu, Q. Zeng, J. Li, X. Hao, A. Ho-Baillie, J. Tang, and M.A. Green, Emerging inorganic compound thin film photovoltaic materials: progress, challenges and strategies. *Mater. Today* 41, 120–142 (2020). <https://doi.org/10.1016/j.mattod.2020.09.002>.
- S.-H. Wei, S.B. Zhang, and A. Zunger, Effects of Ga addition to CuInSe₂ on its electronic, structural, and defect properties. *Appl. Phys. Lett.* 72(24), 3199–3201 (1998). <https://doi.org/10.1063/1.121548>.
- F. Karg, High efficiency CIGS solar modules. *Energy Procedia*. 15, 275–282 (2012). <https://doi.org/10.1016/j.egypro.2012.02.032>.
- B.J. Stanbery, Copper indium selenides and related materials for photovoltaic devices. *Crit. Rev. Solid State Mater. Sci.* 27(2), 73–117 (2002). <https://doi.org/10.1080/20014091104215>.
- P. Jackson, R. Wuerz, D. Hariskos, E. Lotter, W. Witte, and M. Powalla, Effects of heavy alkali elements in Cu(In,Ga)Se₂ solar cells with efficiencies up to 22.6%. *Phys. Status Solidi (RRL) – Rapid Research Letters* 10(8), 583–586 (2016). <https://doi.org/10.1002/pssr.201600199>.
- M.A. Green, E.D. Dunlop, J. Hohl-Ebinger, M. Yoshita, N. Kopidakis, K. Bothe, D. Hinken, M. Rauer, and X. Hao, Solar cell efficiency tables (Version 60). *Prog. Photovoltaics Res. Appl.* 30(7), 687–701 (2022). <https://doi.org/10.1002/ppp.3595>.
- S.N. Alamri, and M.H. Alsadi, Growth of Cu(In, Ga)Se₂ thin films by a novel single flash thermal evaporation source. *J. Taibah Univ. Sci.* 14(1), 38–43 (2019). <https://doi.org/10.1080/16583655.2019.1701389>.
- N.G. Dhere, V.S. Gade, A.H. Jahagirdar, A.A. Kadam, H.P. Patil, and S.S. Kulkarni, Development of sputtering systems for large-area deposition of CuIn_{1-x}GaxSe_{1-y}Sy thin-film solar cells. *J. Vac. Sci. Technol., A: Vac., Surf. Films* 21(4), 1442–1446 (2003). <https://doi.org/10.1116/1.1577128>.
- P.U. Londhe, A.B. Rohom, R. Fernandes, D.C. Kothari, and N.B. Chaurse, Development of superstrate CuInGaSe₂ thin film solar cells with low-cost electrochemical route from nonaqueous bath. *ACS Sustain. Chem. Eng.* 6(4), 4987–4995 (2018). <https://doi.org/10.1021/acssuschemeng.7b04615>.
- Y.M. Shin, C.S. Lee, D.H. Shin, H.S. Kwon, B.G. Park, and B.T. Ahn, Surface modification of CIGS film by annealing and its effect on the band structure and photovoltaic properties of CIGS solar cells. *Curr. Appl. Phys.* 15(1), 18–24 (2015). <https://doi.org/10.1016/j.cap.2014.09.023>.
- L. Zhang, D. Zhuang, M. Zhao, Q. Gong, L. Guo, L. Ouyang, R. Sun, Y. Wei, and S. Zhan, The effects of annealing temperature on CIGS solar cells by sputtering from quaternary target with Se-free post annealing. *Appl. Surf. Sci.* 413, 175–180 (2017). <https://doi.org/10.1016/j.apsusc.2017.03.289>.
- B.T. Jheng, P.T. Liu, M.C. Wu, and H.P.D. Shieh, A non-selenization technology by co-sputtering deposition for solar cell applications. *Opt. Lett.* 37(13), 2760 (2012). <https://doi.org/10.1364/ol.37.002760>.
- P. Jackson, D. Hariskos, R. Wuerz, O. Kiowski, A. Bauer, T.M. Friedlmeier, and M. Powalla, Properties of Cu(In,Ga)Se₂ solar cells with new record efficiencies up to 21.7%. *Phys. Status Solidi (RRL) – Rapid Res. Lett.* 9(1), 28–31 (2015). <https://doi.org/10.1002/pssr.201409520>.
- R. Kannan, J. Keane, and R. Noufi, Properties of high-efficiency CIGS thin-film solar cells. in *Conference Record of the Thirty-first IEEE Photovoltaic Specialists Conference, 2005.* 2005.
- X.L. He, J. Liu, Q.Y. Ye, K. Luo, Y.D. Jiang, C. Liao, L.Q. Ouyang, D.M. Zhuang, J. Mei, and W. Lau, The role of Na incorporation in the low-temperature processed CIGS thin film solar cells using post deposition treatment. *J. Alloy. Compd.* 658, 12–18 (2016). <https://doi.org/10.1016/j.jallcom.2015.10.181>.
- D. Rudmann, D. Bremaud, A.F. da Cunha, G. Bilger, A. Strohm, M. Kaelin, H. Zogg, and A. Tiwari, Sodium incorporation strategies for CIGS growth at different temperatures. *Thin Solid Films* 480, 55–60 (2005). <https://doi.org/10.1016/j.tsf.2004.11.071>.
- Y.B. Kim, Y.N. Lee, S.I. Park, and J.H. Lee, Fabrication and crystal structure analysis of a CIGS solar cell absorber by thermal annealing of sputtered CIG precursors deposited with a Se layer. *Mol. Cryst. Liq. Cryst.* 602(1), 244–250 (2014). <https://doi.org/10.1080/15421406.2014.944785>.
- V. Probst, W. Stetter, W. Riedl, H. Vogt, M. Wendl, H. Calwer, S. Zweigart, K.D. Ufert, B. Freienstein, H. Cerva, and F.H. Karg, Rapid CIS-process for high efficiency PV-modules: development towards large area processing. *Thin Solid Films* 387(1–2), 262–267 (2001). [https://doi.org/10.1016/S0040-6090\(00\)01800-9](https://doi.org/10.1016/S0040-6090(00)01800-9).
- J. Ray, M. Desai, C. Panchal, B. Rehani, and P. Mehta, Effect of rapid thermal annealing of CIGS thin film as an absorber layer. *J. Nano Electron. Phys.* 5(2), 02013 (2013).

20. N.-H. Kim, P.J. Ko, G.-B. Cho, and C.I. Park, Rapid laser annealing of Cu (In, Ga) Se₂ thin films by using a continuous wave Nd: YAG laser ($\lambda_0 = 532$ nm). *J. Korean Phys. Soc.* 70(8), 809–815 (2017).
21. A.B. Rohom, P.U. Londhe, and N.B. Chaurse, Rapid thermal processed CuInSe₂ layers prepared by electrochemical route for photovoltaic applications. *J. Electrochem. Soc.* 165(4), H3051–H3060 (2018). <https://doi.org/10.1149/2.0081804jes>.
22. N. Doebelin and R. Kleeberg, Profex: a graphical user interface for the Rietveld refinement program BGMN. *J Appl Crystallogr.* 48(Pt 5), 1573–1580 (2015). <https://doi.org/10.1107/S1600576715014685>.
23. B.D. Cullity, *Elements of X-ray diffraction* (Reading, Mass: Addison-Wesley Pub. Co, 1956).
24. H.T. Kim, C.D. Kim, and Y.S. Sohn, Properties of CuInGaSe₂ (CIGS) films formed by a rapid thermal annealing process of CuGaSe₂/CuInSe₂ stacked layers. *J. Nanoelectron. Optoelectron.* 10(4), 471–474 (2015). <https://doi.org/10.1166/jno.2015.1784>.
25. M. Soce, A. Ehemba, D. Diallo, I. Wade, and M. Dieng, Determination of the excitonic rydberg energy, the exciton bohr radius for free exciton according to the ratio Ga/(Ga+In) And bandgap energy in the chalcopyrite solar cell. *Int. J. Adv. Res.* 04, 1910–1917 (2016). <https://doi.org/10.21474/IJAR01/1673>.
26. Y.-T. Shih, Y.-C. Tsai, and D.-Y. Lin, Synthesis and characterization of CuIn_{1-x}Ga_xSe₂ semiconductor nanocrystals. *Nanomaterials* 10(10), 2066 (2020).
27. J.I. Pankove, *Optical processes in semiconductors*. Spain, Dover (1975).
28. J. Álvarez-García, B. Barcones, A. Pérez-Rodríguez, A. Romano-Rodríguez, J.R. Morante, A. Janotti, S.H. Wei, and R. Scheer, Vibrational and crystalline properties of polymorphic CuInC₂(C=Se, S)chalcogenides. *Phys. Rev. B.* (2005). <https://doi.org/10.1103/PhysRevB.71.054303>.
29. B. Vidhya, S. Velumani, J.A. Arenas-Alatorre, A. Morales-Acevedo, R. Asomoza, and J.A. Chavez-Carvayar, Structural studies of mechano-chemically synthesized CuIn_{1-x}Ga_xSe₂ nanoparticles. *Mater. Sci. Eng., B* 174(1–3), 216–221 (2010). <https://doi.org/10.1016/j.mseb.2010.03.014>.
30. C.A. Schneider, W.S. Rasband, and K.W. Eliceiri, NIH Image to ImageJ: 25 years of image analysis. *Nat. Methods* 9(7), 671–675 (2012). <https://doi.org/10.1038/nmeth.2089>.
31. C. Adel, B.M. Fethi, and B. Brahim, Effect of annealing under various atmospheres on the properties of electrodeposited CIGS thin films on ITO coated glass substrates. *J. Mater. Sci.: Mater. Electron.* 27(4), 3481–3487 (2016). <https://doi.org/10.1007/s10854-015-4181-y>.
32. B.-S. Ko, S.-J. Sung, D.-H. Kim, D.-H. Lee, and D.-K. Hwang, Effects of annealing on structural and electrical properties of sub-micron thick CIGS films. *Curr. Appl. Phys.* 13, S135–S139 (2013). <https://doi.org/10.1016/j.cap.2013.01.022>.
33. C. Adel, B.M. Fethi, and B. Brahim, Optical and electrical characterization of CIGS thin films grown by electrodeposition route. *Optik* 127(8), 4118–4122 (2016). <https://doi.org/10.1016/j.ijleo.2016.01.115>.
34. Z. Yu, C. Yan, Y. Yan, Y. Zhang, T. Huang, W. Huang, S. Li, L. Liu, Y. Zhang, and Y. Zhao, Effect of annealing temperature on properties of RF sputtered Cu(In, Ga)Se₂ thin films. *Appl. Surf. Sci.* 258(22), 8527–8532 (2012). <https://doi.org/10.1016/j.apsusc.2012.05.034>.

Publisher's Note Springer Nature remains neutral with regard to jurisdictional claims in published maps and institutional affiliations.

Springer Nature or its licensor (e.g. a society or other partner) holds exclusive rights to this article under a publishing agreement with the author(s) or other rightsholder(s); author self-archiving of the accepted manuscript version of this article is solely governed by the terms of such publishing agreement and applicable law.